19th Brazilian Congress of Thermal Sciences and Engineering
November 6th–10th, 2022, Bento Gonçalves - RS - Brazil

ENC-2022-0030
A COMPUTATIONAL ANALYSIS AND VALIDATION OF A LAMINAR-TURBULENT TRANSITION MODEL INCLUDING CROSSFLOW EFFECTS

Aline R. Santos Righi
Instituto Tecnológico de Aeronáutica, 12228-900, São José dos Campos, SP, Brazil
alinerighi29@gmail.com

Gustavo Luiz Olichevis Halila
Embraer S. A., Research & Development, 12227-901, São José dos Campos, SP, Brazil
gustavo.halila@embraer.com.br

João Luiz F. Azevedo
Instituto de Aeronáutica e Espaço, 12228-904, São José dos Campos, SP, Brazil
joaoluiz.azevedo@gmail.com

Abstract. *Computational Fluid Dynamics (CFD) techniques have been used now for many decades in different applications for academic or industrial purposes. However, the appropriate treatment of the laminar-turbulent transition over general configurations is one aspect in the CFD tools that requires further research and development. The approach here uses the Langtry-Menter transition model coupled with the SST model for turbulence closure. The Langtry-Menter model uses two transport equations to correctly predict the laminar-turbulent transition. The original Langtry-Menter transition model is capable of correctly predicting transition due to the amplification of Tollmien-Schlichting waves and bypass transition through empirical correlations. In addition, the Langtry-Menter model was extended in order to account for the crossflow instabilities. The present work is concerned with an empirical correlation based on the surface roughness. The work shows a study of the effects of the freestream turbulence intensity and of the freestream turbulent length scale, as well as considerations regarding the numerical convergence of the solution. The test case addressed here is the flow over a prolate spheroid, which is a well-known case for transition. The fundamental observations include the effects of the freestream turbulent quantities and of the newly added equations in the final solutions.*

Keywords: *Laminar-Turbulent Transition, Langtry-Menter Model, Numerical Convergence, Crossflow Instabilities.*

1. INTRODUCTION

Over the past years, the Computational Fluid Dynamics (CFD) techniques have been used to correctly predict laminar-turbulent transition for academic and industrial purposes. Despite of being improved through out the last decades, the laminar-turbulent transition area still needs some research, specially in the aerospace industry (Versteeg and Malalasekera, 2007). A boundary layer base flow is excited by some external factor in the path to turbulence, for example, roughness, sound, vibration, and freestream turbulence through a mechanism called receptivity. Therefore, there are many different mechanisms leading to laminar-turbulent transition. The amplification Tollmien-Schlichting (TS) waves (Klebanoff *et al.*, 1962), bypass transition (Ghasemi *et al.*, 2014), crossflow vortices (Saric and Dagenhart, 1999), leading edge and flow contamination (Poll, 1978) are, for example, the most common transition mechanisms in the aerospace industry. The laminar-turbulent transition plays an important role in several engineering applications. For example, aircraft configurations not designed to preserve laminar flow may present transitional regions (Halila *et al.*, 2016, 2018), among others. Given that, it is important to correctly predict the transition mechanism.

Through the last decades, many attempts were made aiming the correct prediction of the laminar-turbulent transition. The e^n method (Smith and Gamberoni, 1956; van Ingen, 1956), Large Eddy Simulation (LES) and Direct Numerical Simulations (DNS) (Durbin *et al.*, 2002) are some examples, among others. However, the strategies mentioned before suffer from some limitation. For example, the approaches based on the stability equations connected to an e^n method (Smith and Gamberoni, 1956; van Ingen, 1956) are not compatible with general-purposes CFD methods, because in

these approaches, the stability equations are coupled with a CFD code (Halila *et al.*, 2019), which leads to a complex framework. One more case is the LES method, which is far too costly for engineering applications. The transition process should be viewed inside the range of the Reynolds-averaged Navier-Stokes (RANS) methods. To alleviate the difficulties in using the RANS methods for transition modelings, modified RANS models were proposed with the idea of allowing accurate and inexpensive transitional flow predictions. Usually, these models operate with a standard, fully-turbulent RANS model with one or two additional transport equations based on empirical correlations or local parameters.

Following the modified RANS models, the Langtry-Menter transition model (Langtry and Menter, 2009) (LCTM - Local Correlation-based Transition Model) was proposed. The Langtry-Menter transition is composed of two transport equations and is based only on local variables. In its original form, the Langtry-Menter transition model is capable of correctly predict transition due to the amplification of Tollmien-Schlichting waves and bypass transition, but not transition due to crossflow vortices. Therefore, many extensions of the original model were proposed and published through the last years accounting for new empirical correlations (Langtry *et al.*, 2015; Grabe *et al.*, 2018). The Langtry-Menter transition model is implemented in an in-house code, BRU3D (Bigarella, 2007; Bigarella and Azevedo, 2007; Carvalho *et al.*, 2018). However, transition caused by crossflow vortices was not considered. In this paper, we consider an empirical correlation based on the surface roughness published in Langtry *et al.* (2015), which is implemented in the BRU3D code. We present a study on the freestream parameters and a study on the numerical convergence considering a prolate spheroid test case.

2. METHODS

An in-house developed CFD code, BRU3D (Bigarella, 2007; Bigarella and Azevedo, 2007; Carvalho *et al.*, 2018), is used for the development of the present work. The BRU3D code has been continuously improved by the research group through the years. By now, the code can solve the compressible Euler equations and/or the RANS equations. Many turbulence models are implemented in the code, such as the Shear Stress Transport (SST) (Menter, 1994) model, the Spalart-Allmaras (SA) (Spalart and Allmaras, 1994) model, among others. More recently, the Langtry-Menter laminar-turbulent transition model (Langtry and Menter, 2009) was also implemented. The equations are solved in a discretized cell-centered, finite-volume method for spatial discretization (Hirsh, 1990) for unstructured grids (Bigarella, 2007; Bigarella and Azevedo, 2009). Further information on the details of the spatial discretization approach adopted and the numerical schemes used in the present work can be found in Refs. Bigarella and Azevedo (2009); Carvalho (2018).

2.1 The Shear Stress Transport Turbulence Model

In our implementation, the Langtry-Menter $\gamma - Re_\theta$ transition model (Langtry and Menter, 2009) is coupled to the SST turbulence model (Menter, 1994). The SST model is based on the Boussinesq hypothesis, in which the eddy viscosity, μ_t, is used as a means to represent the Reynolds stress tensor terms. The SST model uses a blending function, F1, to combine the advantages of the k-ϵ and the k-ω models. The blending function, F1, activates the k-ω model in the near wall region, and the k-ϵ model for the rest of the flow. The SST model is composed of two equations. The first equation is for the turbulent kinetic energy, k, given by

$$\frac{\partial(\rho k)}{\partial t} + \frac{\partial(\rho u_j\, k)}{\partial x_j} = P_k - D_k + \frac{\partial}{\partial x_j}\left[\left(\mu + \frac{\mu_t}{\sigma_k}\right)\frac{\partial k}{\partial x_j}\right], \tag{1}$$

where ρ is the density, u_j represents the velocity vector components, P_k is the production term and D_k is the destruction term, μ is the molecular dynamic viscosity, μ_t is the eddy viscosity, and $\sigma_k = 0.85$. The second equation is for the turbulence frequency, ω, given by

$$\frac{\partial(\rho\omega)}{\partial t} + \frac{\partial(\rho u_j\omega)}{\partial x_j} = \frac{\gamma}{\nu_t}P_\omega - \beta\rho\omega^2 + \frac{\partial}{\partial x_j}\left[\left(\mu + \frac{\mu_t}{\sigma_k}\right)\frac{\partial\omega}{\partial x_j}\right] + (1-F_1)2\rho\sigma_{\omega 2}\frac{1}{\omega}\frac{\partial k}{\partial x_j}\frac{\partial\omega}{\partial x_j}, \tag{2}$$

where P_ω is the production term, $\beta = 0.09$, $\gamma = \frac{\beta_1}{\beta*} - \frac{\sigma_{\omega 1}\kappa^2}{\sqrt{\beta*}}$ with $\beta_1 = 0.075$, $\sigma_{\omega 1} = 0.5$ and $\kappa = 0.41$, and $\sigma_{\omega 2} = 0.856$.

The production term for the kinetic energy equations, P_k, is

$$P_k = \min\left(\mu_t S^2, 10D_k\right), \tag{3}$$

where S is the strain rate magnitude, given by

$$S = \sqrt{2S_{ij}S_{ij}}. \tag{4}$$

The destruction term for the kinetic energy equation, D_k, is

$$D_k = \beta^*\rho\omega k. \tag{5}$$

The blending function, F_1, is

$$F_1 = \tanh\left(\min\left(\max\left(\frac{\sqrt{k}}{\beta * \omega y}\,;\,\frac{500\nu}{y^2\omega}\right)\,;\,\frac{4\rho\sigma_{\omega 2}k}{CD_{k\omega}y^2}\right)\right)^4\,, \tag{6}$$

where y is the distance from the field point to the nearest wall, and

$$CD_{k\omega} = \max\left(2\rho\sigma_{\omega 2}\frac{1}{\omega}\frac{\partial k}{\partial x_j}\frac{\partial \omega}{\partial x_j}\,;\,1\times 10^{-10}\right)\,. \tag{7}$$

The turbulent viscosity is calculated as follows

$$\mu_t = \min\left(\frac{\rho k}{\omega}\,;\,\frac{a_1\rho k}{SF_2}\right)\,, \tag{8}$$

where $a_1 = 0.31$. The F_2 term is a blending function given by

$$F_2 = \tanh\left\{\max\left(2\frac{\sqrt{k}}{\beta * \omega y}\,;\,\frac{500\mu_t}{\rho y^2\omega}\right)\right\}^2\,. \tag{9}$$

Further information on the SST model can be found in Ref. Menter (1994).

2.2 Langtry-Menter Transition Model Standard Formulation

In our implementation, the Langtry-Menter $\gamma - Re_{\theta_t}$ transition model (Langtry and Menter, 2009) is coupled with the SST turbulence model (Menter, 1994). The model is composed of two transport equations in addition to the equations for the SST model. The Langtry-Menter transition model is based only on local variables and is compatible with modern CFD codes. In the Langtry-Menter model, the strain rate Reynolds number, which is a local variable, maps the momentum-thickness Reynolds number, which is nonlocal and plays an important role in transition prediction.

The first transport equation of the Langtry-Menter model is for the intermittency, γ, which is used to trigger the SST source terms, and is given by

$$\frac{\partial(\rho\gamma)}{\partial t} + \frac{\partial(\rho u_j\gamma)}{\partial x_j} = P_\gamma - E_\gamma + \frac{\partial}{\partial x_j}\left[\left(\mu + \frac{\mu_t}{\sigma_f}\right)\frac{\partial\gamma}{\partial x_j}\right]\,, \tag{10}$$

where ρ is the density, u_j represents the velocity vector components, P_γ is the intermittency source term, E_γ is the destruction-relaminarization source term, μ is the molecular dynamic viscosity, μ_t is the eddy viscosity and $\sigma_f = 1.0$. The intermittency represents the probability of a fluid cell to be turbulent.

The second transport equation represents the momentum thickness Reynolds number, $\tilde{R}e_{\theta_t}$, which is written for the transition onset, and is given by

$$\frac{\partial\left(\rho\tilde{R}e_{\theta_t}\right)}{\partial t} + \frac{\partial\left(\rho u_j\tilde{R}e_{\theta_t}\right)}{\partial x_j} = P_{\theta_t} + \frac{\partial}{\partial x_j}\left[\sigma_{\theta_t}\left(\mu + \mu_t\right)\frac{\partial\tilde{R}e_{\theta_t}}{\partial x_j}\right]\,, \tag{11}$$

where P_{θ_t} is the source term and $\sigma_{\theta_t} = 2.0$ controls the diffusion coefficient. The Reynolds number based on the momentum-thickness represents a sensor responsible for triggering the transition process, because $\tilde{R}e_{\theta_t}$ indicates the point where the transition begins.

The Langtry-Menter model couples the intermittency function with the SST model to activate the turbulent kinetic energy,

$$\frac{\partial(\rho k)}{\partial t} + \frac{\partial(\rho u_j k)}{\partial x_j} = \tilde{P}_k - \tilde{D}_k + \frac{\partial}{\partial x_j}\left[\left(\mu + \sigma_k\mu_t\right)\frac{\partial k}{\partial x_j}\right]\,, \tag{12}$$

$$\tilde{P}_k = \gamma_{eff}P_k, \tag{13}$$

$$\tilde{D}_k = \min\left(\max\left(\gamma_{eff}\,,\,0.1\right)\,,\,1.0\right)D_k\,, \tag{14}$$

$$R_y = \frac{\rho y\sqrt{k}}{\mu}\,, \tag{15}$$

$$F_3 = \exp\left[-\left(\frac{R_y}{120}\right)^8\right] , \tag{16}$$

$$F_1 = \max(F_{1orig}, F_3) , \tag{17}$$

where $\tilde{P}_k$ and $\tilde{D}_k$ are the original production and destruction terms of the SST model, $\gamma_{eff}P_k$ includes the separation effects in the formulation, and F_{1orig} is the original SST blending function.

The original Langtry-Menter transition model is able to predict transition triggered by the amplification of Tollmien-Schlichting waves and bypass transition. Further information and the empirical correlations can be found in the literature (Langtry and Menter, 2009).

2.3 Empirical Correlation Based on the Surface Roughness

The Langtry-Menter transition model was extended with a new empirical correation Langtry *et al.* (2015) in order to correctly prediction transition due to stationary crossflow transition. The new empirical correlation for crossflow effects is based on the streamwise vorticity ($\Omega_{\text{Streamwise}}$), alternatively known as helicity, as an indicator of the local crossflow strength in the boundary layer, defined as follows

$$\vec{U} = \left(\frac{u}{\sqrt{u^2+v^2+w^2}}, \frac{v}{\sqrt{u^2+v^2+w^2}}, \frac{w}{\sqrt{u^2+v^2+w^2}}\right) , \tag{18}$$

$$\vec{\Omega} = \left(\frac{\partial w}{\partial y} - \frac{\partial v}{\partial z}, \frac{\partial u}{\partial z} - \frac{\partial w}{\partial x}, \frac{\partial v}{\partial x} - \frac{\partial u}{\partial y}\right) , \tag{19}$$

$$\Omega_{Streamwise} = |\vec{U} \cdot \vec{\Omega}|. \tag{20}$$

In order to non-dimensionalize $\Omega_{Streamwise}$ into a measure of the crossflow strength, and to build an empirical correlation based on $\mathrm{H}_{crossflow}$, the non-dimensional parameter is defined as

$$H_{Crossflow} = \frac{y\Omega_{Streamwise}}{U}, \tag{21}$$

as the crossflow strength indicator, where y is the distance to the nearest wall, and U is the magnitude of the nondimensional velocity vector defined in Eq. (18). The new empirical correlation for crossflow effects accounts for the surface roughness on the transition momentum thickness Reynolds number,

$$Re_{SCF} = \frac{\theta_t \rho \left(\frac{U}{0.82}\right)}{\mu} = -35.088 \ln\left(\frac{h}{\theta_t}\right) + 319.51 + f(+\Delta H_{crossflow}) - f(-\Delta H_{crossflow}) , \tag{22}$$

where $f(+\Delta H_{crossflow})$ and $f(-\Delta H_{crossflow})$ are a shift up or down depending on the local crossflow strength, θ_t is the momentum thickness, U is the velocity magnitude, and ρ is the density. The crossflow effect is implemented as a stationary crossflow sink term D_{SCF} in the Re_{θ_t} transport equation as

$$\frac{\partial(\rho\tilde{R}e_{\theta_t})}{\partial t} + \frac{\partial(\rho u_j \tilde{R}e_{\theta_t})}{\partial x_j} = P_{\theta_t} + D_{SCF} + \frac{\partial}{\partial x_j}\left[\sigma_{\theta_t}(\mu+\mu_t)\frac{\partial \tilde{R}e_{\theta_t}}{\partial x_j}\right] , \tag{23}$$

where

$$D_{SCF} = c_{\theta_t}\frac{\rho}{t}c_{crossflow}\min\left(Re_{SCF} - \tilde{R}e_{\theta_t}, 0.0\right)(F_{\theta_t 2}) , \tag{24}$$

$$F_{\theta_t 2} = \min\left(F_{wake}e^{-\left(\frac{y}{\delta}\right)^4}, 1.0\right) , \tag{25}$$

where $c_{crossflow} = 0.6$, and $F_{\theta_t 2}$ confines the crossflow sink term D_{SCF} so that it is only activated inside the boundary layer. Further information on the details of the above empirical correlation for the prediction of crossflow instabilities can be found in the literature (Langtry *et al.*, 2015).

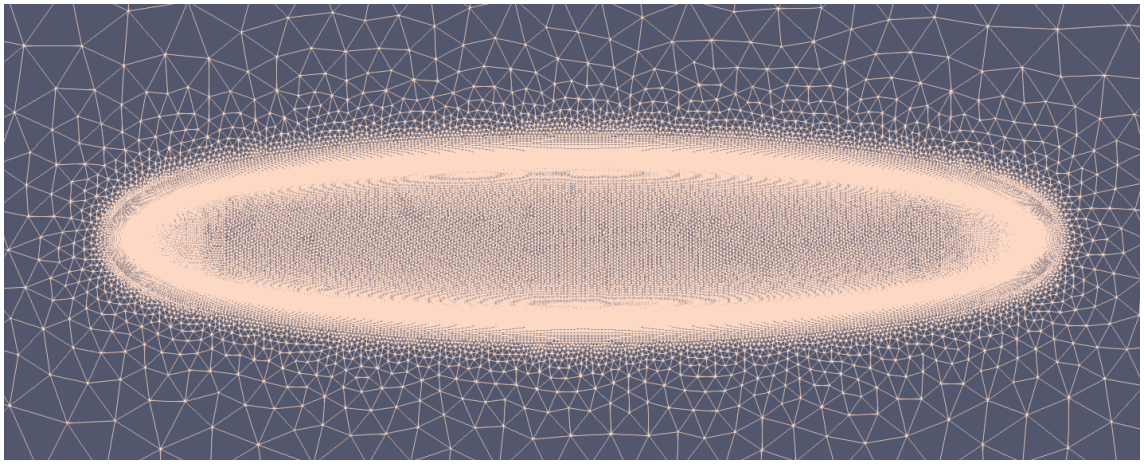

Figure 1. Unstructured, 128×20000 prolate spheroid grid.

3. RESULTS

In the present work, we discuss some results obtained for a prolate spheroid test case which is a well-known case for simulations of transitional flows. A picture of the unstructured grid is available in Fig. 1. The surface grid represents only the right half of the geometry, which requires a symmetry-plane boundary condition. The grid level is 128×20000, with 128 prism layers in the wall normal direction and $20,026$ surface nodes, leading to a $2,715,698$ total nodes (Coder, 2018). The wall normal direction has $60 - 100$ nodes located inside the boundary layer, resulting in a $y^+(1) = 1.0$ in the cell next to the wall.

There are three cases considered here for transition due to the amplification of TS waves. The experimental study for the 6:1 prolate spheroid test case was performed at the low speed wind tunnel of the DLR in Göttingen (Kreplin *et al.*, 1985). The freestream turbulence intensity in the wind tunnel is $Tu_i \approx 0.1\%$ considering different test conditions for transition caused by the amplification of TS waves, the amplification of TS waves and crossflow instabilities, and crossflow instabilities alone. The transition front extracted from the experimental results obtained for the skin friction coefficients, c_f, contours are used to confront our numerical results through the black line in our own plots of the c_f contours. A few operational test conditions for computational simulations were performed and published in Grabe and Krumbein (2013). Operational test conditions are 10-degree angle of attack, a Mach number of 0.03, and a 1.5×10^6 Reynolds number. In the computations, in order to get the appropriate turbulence level in the vicinity of the spheroid, the reference freestream turbulence intensity at the farfield was set to $Tu_i = 1\%$. We compare our numerical results with the numerical data obtained in Grabe and Krumbein (2013). The transition front extracted from the reference computational results is indicated by the white line in our own plots of the skin friction coefficient contours. To summarize, our reference freestream values for the cases considered are presented in Tab. 1.

Table 1. Reference freestream values for the three cases with transition due to amplification of TS waves.

Case	α (deg)	Re	Mach	Tu_i (%)	μ_t/μ_{ref}
Case A	10	1.5×10^6	0.14	0.2	100
Case B	10	1.5×10^6	0.14	0.2	10
Case C	10	1.5×10^6	0.14	0.2	50

Figure 2 depicts our numerical results for Case A. The region on the surface of the prolate spheroid where the c_f contours shift from blue to yellow represents the transition location. Comparing our numerical results with the experimental and numerical data, represented by the black and the white lines in the figure, from the references (Kreplin *et al.*, 1985; Grabe and Krumbein, 2013), we can see good agreement between numerical and experimental results. We can also observe that the black and white lines are, essentially, on top of one another.

Figure 3 shows the numerical results for Case B considering a viscosity ratio, μ_t/μ_{ref}, of 10. Case B considers the smallest value of μ_t/μ_{ref} in our numerical simulations. Therefore, the values of c_f observed in the post-transition region are smaller than those seen in the same region in Case A. Even more, one can see that the transition front and the values of c_f in the turbulent regions are smaller in the computations for Case B than in those for Case A, or in the reference contours. However, the position of the transition front seems to be in good agreement with both the experimental and computational reference results.

Case C, Fig. 4, is for a value of μ_t/μ_{ref} intermediary among the studied cases. The values of c_f observed for Case C in the post-transition region are smaller than those seen in this region in Case A, but the values in the same region

are larger than in Case B. Cases B and C show that there are some small discrepancies between the computational and experimental references (Kreplin *et al.*, 1985; Grabe and Krumbein, 2013), as one can see that the black lines extends slightly upstream than the white line in both test cases. The discrepancy observed between our numerical results and the results from the references (Kreplin *et al.*, 1985; Grabe and Krumbein, 2013) appeared after smaller values for the physical parameter of the viscosity ratio were tested. The region of turbulent flow is smaller than expected. However, in the area of increasing c_f, indicating the transition region, our numerical results are in good agreement when confronting with the experimental and numerical results from the references.

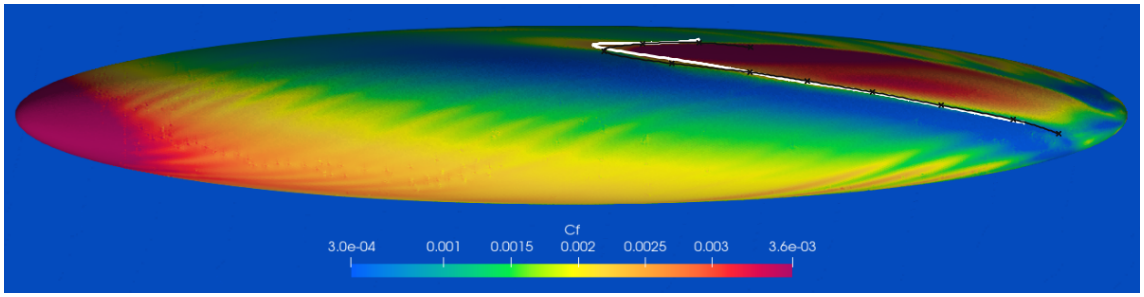

Figure 2. Skin friction coefficient contours for Case A.

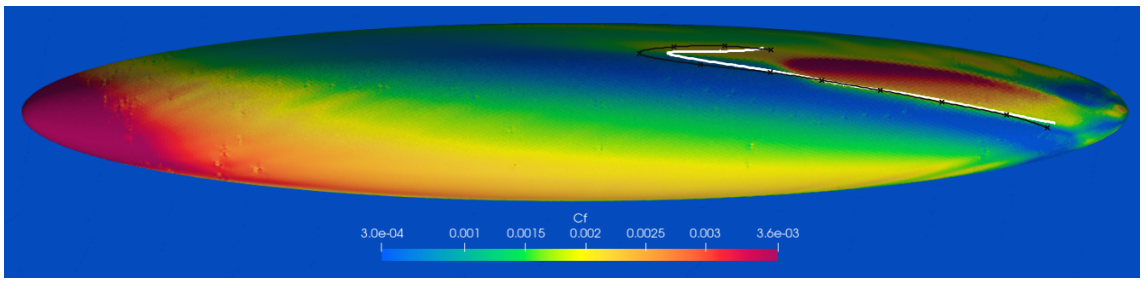

Figure 3. Skin friction coefficient contours for Case B.

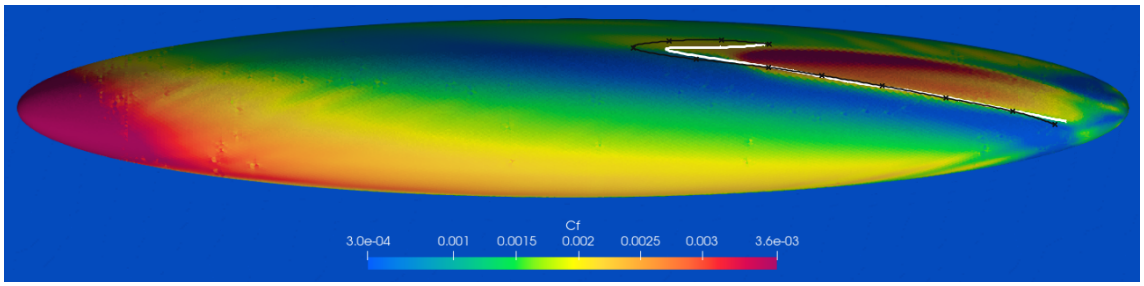

Figure 4. Skin friction coefficient contours for Case C.

Figure 5 shows the residual convergence for the L_∞ norms for Cases A, B and C. The curves present the history of the L_∞ norm for the residuals for the two quantities being solved by the Langtry-Menter transition model, γ and Re_{θ_t} for the three cases. Gamma1, Gamma2 and Gamma3 stand for the residual curves for the intermittency variable for Cases A, B and C, respectively. Following the same idea, ReThetaT1, ReThetat2 and ReThetat3 are the curves for the numerical residuals of the momentum thickness Reynolds number variable for Cases A, B and C, respectively. One can see that Gamma1 and ReThetaT2 have lower convergence rates comparing with the other curves. The remaining curves indicate similar convergence rates.

We also include results for the implemented empirical correlation for stationary crossflow transition found in Langtry *et al.* (2015). The numerical simulation is performed for a prolate spheroid test case, which is a well-known test case for transition due to stationary crossflow transition. The grid for the stationary crossflow transition computation is the same as in Fig. 1. The investigation includes the impacts of the reference freestream variables on the numerical results. As mentioned before, the experimental results obtained in Kreplin *et al.* (1985) are used to confront our numerical results. The transition front is extracted from the reference results and it is represented by the black line in our own c_f plots. Moreover, the result is further compared to the numerical data obtained in Langtry *et al.* (2015) for the c_f contours with the unstructured BCFD code, and with the OVERFLOW code. In Langtry *et al.* (2015), the authors considered a 6.5×10^6 Reynolds number, a 15-degree angle of attack, a 0.14 Mach number, a 0.1% freestream turbulence intensity, a μ_t/μ_{ref}

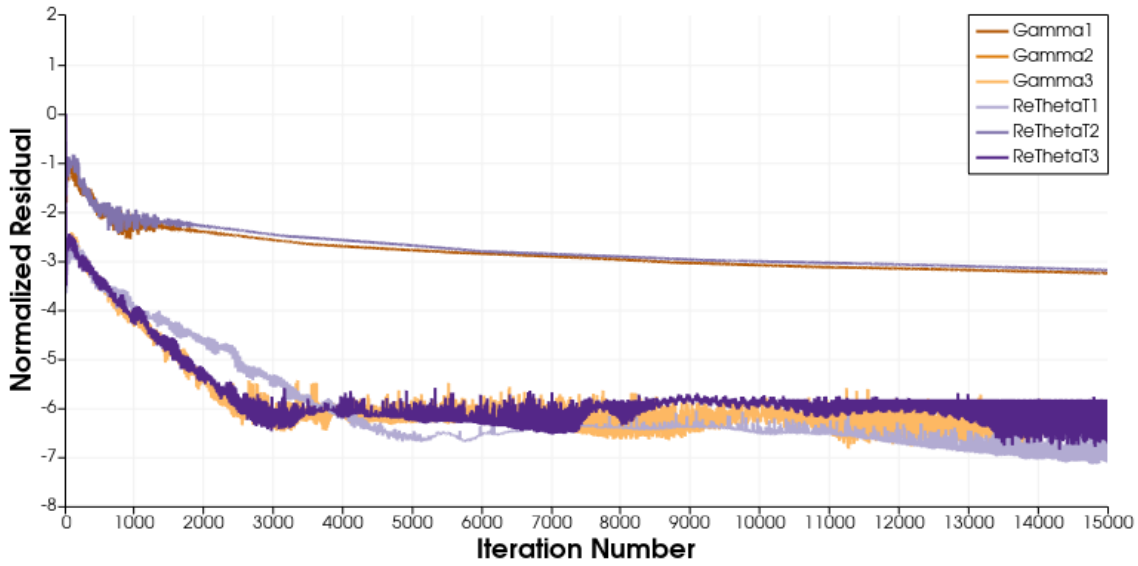

Figure 5. Residual convergence for the two quantities being solved by the Langtry-Menter model for three test cases addressed in this work.

of 10, and surface roughness of 3.3μm. According to Langtry *et al.* (2015), good agreement between their numerical results and the experimental data is observed. The results obtained for the c_f contours in Langtry *et al.* (2015) are used for comparison of our calculations. In the following figures, the yellow line superimposed in our own plots represents the transition front extracted from the reference results for the c_f contours. Table 2 presents the flow conditions for our numerical simulation.

Table 2. Flow conditions and freestream turbulent variables for stationary crossflow vortices test case.

Case	α	Re	Mach	h (μm)	T_u	μ_t/μ_{ref}
Case D	15 deg	6.5×10^6	0.14	3.3	0.1%	10

In the previous cases with a 10-degree angle of attack and a lower Reynolds number of 1.5×10^6, the transition process was controlled by the amplification of Tollmien-Schlichting waves. For a 15-degree angle of attack and a 6.5×10^6 Reynolds number, the transition process is controlled purely by crossflow instabilities. Figure 6 depicts the skin friction coefficient contours for Case D.

In Fig. 6, the regions on the surface of the prolate spheroid where the contours shift from blue to red represent the transition location. We observe a discrepancy in our numerical results when compared to the experimental data and the numerical results from the reference. In our numerical results, the format and location of the transition front are different when comparing with the black and the yellow lines from the experimental and numerical data provided by Kreplin *et al.* (1985) and by Langtry *et al.* (2015), respectively. The present calculations are not able to predict the transition front location in the same position as the reference data, especially in the pressure side of the body. The transition front location in the suction side of the body is actually predicted quite well by our calculations. The strong influence of crossflow on transition for this case places a strain on the predictive capability of CFD based transition models, leading to pronounced discrepancies between the prediction and measurement as shown by the results (Coder, 2018). Therefore, there are more tests being performed in order to fully understand our numerical results. We understand that, adding more nonlinearities to the code, the numerical results can change from solver to solver, and further investigations are necessary.

Figure 7 shows the normalized residual convergence for the L_∞ norms for Case D considering the crossflow effects. The curves represent the quantities being solved for the Langtry-Menter transition model, the intermittency, γ, and the transition momentum thickness Reynolds number, Re_{θ_t}. The curve for γ has a better convergence rate than the curve for the Re_{θ_t} variable. Similar behavior was observed before. We also observed that, for the crossflow test case, more iterations were necessary in order to achieve some convergence for the Re_{θ_t} variable. Such behavior is also different from the one observed for the standard Langtry-Menter transition model.

4. CONCLUSIONS

The present study is concerned with the use of the Langtry-Menter transition model in its original formulation and the extended version for transition due to stationary crossflow vortices. We focus on the prolate spheroid test case, which is

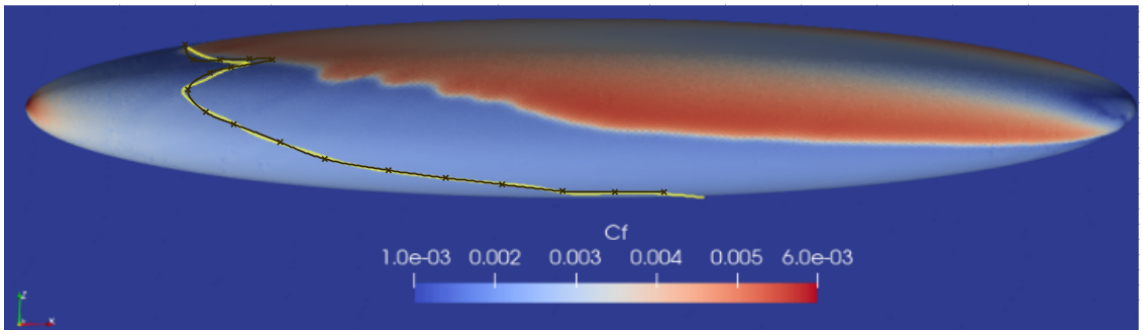

Figure 6. Skin friction coefficient contours for Case D with the inclusion of the crossflow transition effects.

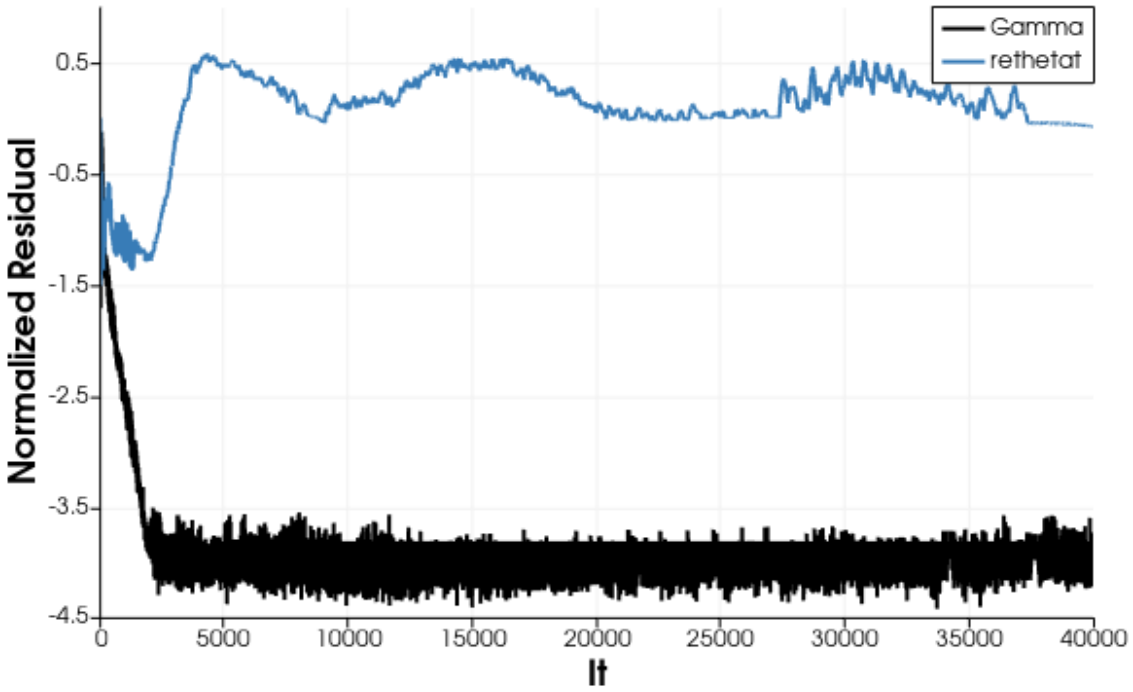

Figure 7. Residual convergence for the two quantities being solved for the Langtry-Menter model for Case D.

a well-known test case for laminar-turbulent transition, analyzing the c_f contours for the transition location. Three test cases are studied for transition due to the amplification of Tollmien-Schlichting waves. Case A is confronted with the experimental and numerical data, and we observe good agreement. Cases B and C are concerned with the impacts on the numerical solutions for different reference values of dynamic eddy viscosity and dynamic molecular viscosity ratio. We observe and analyze the impacts on the skin friction coefficient contours for the three cases. The main observation is for Case B where the smallest value for the viscosity ratio is considered. Case B has shown a region of turbulence flow which is smaller than the corresponding region observed in the results found in the references. Moreover, the transition front on the geometry surface is also smaller than in Case A, Case C, and the references. Furthermore, we also analyze the numerical convergence of the two quantities being solved by the Langtry-Menter transition model for the three cases.

The empirical correlation for the extended Langtry-Menter version is implemented in the BRU3D code. We start our numerical tests for stationary crossflow transition by analyzing the values on the contours of c_f. We observe some discrepancies between our numerical transition location compared to the transition location from the data available in the literature and the experimental results. However, there is some agreement on the position of the transition front in the suction side of the body and the transition front topology is similar to the results obtained by other research groups. It is worth mentioning that adding more equations, and for consequence more nonlinearities to the model, can affect the results from solver to solver, and further investigations are being made. Finally, we analyze the numerical convergence of the quantities being solved by the Langtry-Menter transition model crossflow test case.

5. ACKNOWLEDGEMENTS

The authors gratefully acknowledge the support provided by Fundação de Amparo à Pesquisa do Estado de São Paulo, FAPESP, through a doctoral scholarship for the first author under Grant No. 2021/00031-0. The simulations in the present work would not be possible without the computational resources from the Center for Mathematical Sciences Applied to Industry (CeMEAI), funded by FAPESP under the Research Grant No. 2013/07375-0. Additional support to the third author under the FAPESP Research Grant No. 2013/07375-0 is also gratefully acknowledged. Further support for the present research was provided by Conselho Nacional de Desenvolvimento Científico e Tecnológico, CNPq, under the Research Grant No. 309985/2013-7.

6. REFERENCES

Bigarella, E.D.V., 2007. *Advanced Turbulence Modelling for Complex Aerospace Applications*. Ph.D. thesis, Instituto Tecnológico de Aeronáutica, São José dos Campos, Brazil.

Bigarella, E.D.V. and Azevedo, J.L.F., 2007. "Advanced eddy-viscosity and Reynolds-stress turbulence model simulations of aerospace applications". *AIAA Journal*, Vol. 45, No. 10, pp. 2369–2390.

Bigarella, E.D.V. and Azevedo, J.L.F., 2009. "A unified implicit CFD approach for turbulent-flow aerospace-configurations simulations". In *Proceedings of the 47th AIAA Aerospace Sciences Meeting Including the New Horizons Forum and Aerospace Exposition,* AIAA Paper No. 2009-1473. Orlando, FL.

Carvalho, L.M.M.O., 2018. *Numerical Study of Transitional Flows Over Aerospace Configurations*. Master's thesis, Instituto Tecnológico de Aeronáutica, São José dos Campos, Brasil.

Carvalho, L.M.M.O., da Silva, R.G. and Azevedo, J.L.F., 2018. "Numerical study of transitional flows over aerospace configurations". In *Proceedings of the 2018 AIAA Applied Aerodynamics Conference, AIAA Aviation Forum,* AIAA Paper No. 2018-4209.

Coder, J.G., 2018. "Standard test cases for transition model verification and validation in computational fluid dynamics". In *Proceedings of the 2018 AIAA Aerospace Sciences Meeting, AIAA SciTech Forum,* AIAA Paper No. 2018-0029. Kissimmee, FL.

Durbin, P., Jacobs, R. and Wu, X., 2002. *DNS of Bypass Transition*, Cambridge University Press, Cambridge, p. 449–463.

Ghasemi, E., McEligot, D., Nolan, K., Crepeau, Siahpush, A., Budwig, R. and Tokuhiro, A., 2014. "Effects of adverse and favorable pressure gradients on entropy generation in a transitional boundary layer region under the influence of freestream turbulence". *International Journal of Heat and Mass Transfer*, Vol. 77, pp. 475–488.

Grabe, C. and Krumbein, A., 2013. "Transition transport modeling for three-dimensional aerodynamic configurations". *Journal of Aircraft*, Vol. 50, No. 5, pp. 1535–1539.

Grabe, C., Shengyang, N. and Krumbein, A., 2018. "Transport modeling for the prediction of crossflow transition". *AIAA Journal*, Vol. 56, pp. 3167–3178.

Halila, G.L.O., Bigarella, E.D.V., Antunes, A.P. and Azevedo, J.L.F., 2018. "An efficient setup for freestream turbulence on transition prediction over aerospace configurations". *Aerospace Science and Technology*, Vol. 81, pp. 259–271.

Halila, G.L.O., Bigarella, E.D.V. and Azevedo, J.L.F., 2016. "A numerical study on transitional flows using a correlation-based transition model". *Journal of Aircraft*, Vol. 53, No. 4, pp. 922–941.

Halila, G.L.O., Chen, G., Shi, Y., Fidkowski, K.J., Martins, J.R.R.A. and Mendonça, M., 2019. "High-Reynolds number transitional flow prediction using a coupled discontinuous-Galerkin RANS PSE framework". *Aerospace Science and Technology*, Vol. 91, pp. 321–336.

Hirsh, C., 1990. *Numerical Computation of Internal and External Flows*. Wiley, New York.

Klebanoff, P.S., Tidstrom, K.D. and Sargent, L.M., 1962. "The three-dimensional nature of boundary layer instability". *Journal of Fluid Mechanics*, Vol. 12, pp. 1–24.

Kreplin, H.P., Vollmers, H. and Meier, H.U., 1985. "Wall shear stress measurements on an inclined prolate spheroid in the DFVLR 3m x 3m low speed wind tunnel, Göttingen". Technical Report IB-22-84-A-33, DFVLR-AVA, Göttingen.

Langtry, R.B., Sengupta, K., Yeh, D.T. and Dorgan, A.J., 2015. "Extending the γ - Re local correlation based transition model for crossflow effects". In *Proceedings of the 2015 AIAA Fluid Dynamics Conference, AIAA Aviation Forum,* AIAA Paper No. 2015-2474. Dallas, TX.

Langtry, R.B. and Menter, F.R., 2009. "Correlation-based transition modeling for unstructured parallelized computational fluid dynamics codes". *AIAA Journal*, Vol. 47, No. 12, pp. 2894–2906.

Menter, F.R., 1994. "Two-equation eddy viscosity turbulence models for engineering applications". *AIAA Journal*, Vol. 32, No. 8, pp. 1598–1605.

Poll, D.I.A., 1978. "Some aspects of the flow near a swept attachment line with particular reference to boundary layer transition". College of Aeronautics TR 7805, College of Aeronautics, Cranfield, England, UK.

Saric, W.S. and Dagenhart, J.R., 1999. "Crossflow stability and transition experiments in swept-wing flow". NASA TP-1999-209344, NASA, Hampton, VA.

Smith, A.M.O. and Gamberoni, N., 1956. "Transition, pressure gradient and stability theory". Douglas Aircraft Company

Report ES 26388, Douglas Aircraft Company, Long Beach, CA.

Spalart, P.R. and Allmaras, S.R., 1994. "A one-equation turbulence model for aerodynamic flows". *La Recherche Aerospatiale*, Vol. 1, pp. 5–21.

van Ingen, L.J., 1956. "A suggested semi-empirical method for the calculations of the boundary layer transition region". Dept. Aerospace Engineering VTH 74, University of Delft, Delft, The Netherlands.

Versteeg, K.H. and Malalasekera, W., 2007. *An Introduction to Computational Fluid Dynamics*. Pearson Education Limited, Harlow, England, 2nd edition.

7. RESPONSIBILITY NOTICE

The authors are solely responsible for the printed material included in this paper.